Quantum localization in the high-frequency limit

Emil Persson,[1] Shuhei Yoshida,[1] Xiao-Min Tong,[2] Carlos O. Reinhold,[3,4] and Joachim Burgdörfer[1,4]
[1]*Institute for Theoretical Physics, Vienna University of Technology, A 1040 Vienna, Austria*
[2]*Kansas State University, Manhattan, Kansas 66506*
[3]*Physics Division, Oak Ridge National Laboratory, Oak Ridge, Tennessee 37831-6372*
[4]*Department of Physics, University of Tennessee, Knoxville, Tennessee 37996-1200*
(Received 12 June 2002; published 10 October 2002)

The quantum localization of the periodically kicked Rydberg atom in the limit of high frequencies ν is studied. We show that the quantum suppression of fast chaotic ionization as predicted by classical dynamics persists as $\nu\rightarrow\infty$. Properties of localization in the regime of strong coupling to the continuum due to one-photon transitions are discussed. For the unidirectionally kicked atom, the *high-frequency* limit of localization is determined by the *zero-frequency* Stark Hamiltonian. The persistence of quantum localization due to interference of classical trajectories can be understood in terms of smearing out of the instabilities at finite $\hbar$. Unstable trajectories whose action differs from each other and from Stark orbits in less than $\hbar$ contribute to quantum localization rather than to chaotic ionization.

DOI: 10.1103/PhysRevA.66.043407 PACS number(s): 32.80.Rm, 05.45.Mt, 32.60.+i

I. INTRODUCTION

The quantum mechanics of simple but classically chaotic systems with few degrees of freedom has become the focus of many investigations. Both time-independent systems such as the hydrogen atom in a strong magnetic field [1,2] as well as time-dependent, driven systems such as the kicked rotor [3,4] or the hydrogen atom in a harmonic driving field [5–8] are prime candidates. More recently, the ''kicked'' Rydberg atom, that is, the hydrogen atom perturbed by a periodic sequence of ultrashort pulses, has been experimentally realized [9,10]. The experimental study of this previously theoretically investigated system [11–14] has stimulated further investigations [15–19]. One of the remarkable features of discordance between quantum and classical dynamics is the suppression of classical diffusion of phase space flow due to destructive interference. This effect, usually referred to as quantum localization, has been first predicted for the kicked rotor [3] and shown for this system to be closely connected to the Anderson localization problem in disordered systems [4,20]. The kicked rotor has been meanwhile experimentally realized by trapping atoms in a standing laser field [21]. Quantum localization also has been extensively analyzed for the microwave driven Rydberg atom [5,7,22] for scaled frequencies of the driving field (in units of the orbital period) $\nu_0 \gtrsim 1$. More recently, we found first evidence for quantum localization for the unidirectionally periodically kicked Rydberg atom [23].

The regime of high frequencies is of interest for several reasons: For large ν_0, the one-photon transition leads to direct ionization. For the microwave ionization problem, it was therefore concluded that in this regime of single photoionization, $\nu_0 \gtrsim n_i/2$ (n_i is the initial principal quantum number) ''all vestiges of classical motion have disappeared'' [5,24]. Moreover, because of the simultaneous presence of all higher harmonics, the kicked system is, unlike harmonically driven systems, characterized by a very strong coupling to the continuum. The localized wave packets, if existent at all, must contain a considerable admixture of continuum states, a feature absent for the kicked rotor or harmonically driven systems. In the following we will show that for the kicked Rydberg atom classical ionization via chaotic diffusion continues to dominate quantum ionization and the suppression of classical ionization by quantum localization persists up to very high frequencies.

Identification of quantum localization in numerical solutions of the Schrödinger equation beyond the phenomenological observation of an enhanced stability against ionization compared to its classical counterpart requires the analysis of the Floquet spectrum of the periodically driven system [25]. As localization at high frequencies inevitably involves coupling to continuum states, the imaginary part of the Floquet eigenvalues provides clues as to the properties of localization. Remarkably, we find that for the unidirectionally kicked atom the Floquet width of localized states converges in the high-frequency limit to that of zero-frequency Stark states. We present a simple semiclassical argument for the high-frequency limit of localized states in terms of the quantum uncertainty which allows unstable periodic orbits to retrace Stark orbits and, thereby, provide for the interferences causing localization.

The plan of the paper is as follows: In Sec. II we briefly describe the present method employed in the solution of the time-dependent Schrödinger equation (TDSE). Numerical results for the time-development of the quantum and of the classical system will be shown in Sec. III and the Floquet states will be studied in Sec. IV. Classical-quantum correspondence at high frequencies is discussed in Sec. V, followed by a short summary.

II. GENERALIZED PSEUDOSPECTRAL METHOD

The periodically kicked Rydberg atom is experimentally realized by exposing alkali atoms initially prepared in a high lying Rydberg state $(n_i p)$ to a train of equispaced half-cycle pulses $F(t)$ [10]. If the duration of a pulse is much shorter than the orbital period $T_n = 2\pi n^3$ (a.u.) of the Rydberg atom

with principal quantum number n, each pulse simply transfers a momentum

$$\Delta\vec{p} = -\int \vec{F}(t)dt \tag{1}$$

to the electron. Thus a sequence of half-cycle pulses can be adequately approximated by a sequence of δ functions

$$\vec{F}(t) = \Delta\vec{p}\sum_{k=1}^{K} \delta\left(t - \left(k - \frac{1}{2}\right)T\right), \tag{2}$$

where K is the number of kicks and T the period between kicks. We study the one-dimensional (1D) kicked atom described by the Hamiltonian (in atomic units)

$$H(t) = H_{\rm at} + V(t), \tag{3}$$

where

$$H_{\rm at} = \frac{p^2}{2} - \frac{1}{q}, \tag{4}$$

and

$$V(t) = -q\Delta p\sum_{k=1}^{K} \delta\left(t - \left(k - \frac{1}{2}\right)T\right). \tag{5}$$

Here p and $q(>0)$ are the momentum and position of the electron in the rest frame of the nucleus, respectively. Note that we placed the kicks at the midpoint of the period T, i.e., the first kick comes at $t = T/2$. The restriction of the present calculations to a 1D model serves the purpose to achieve fully converged numerical results with the high-energy continuum accurately represented. We note, however, that we have observed qualitatively similar results in numerical solutions for the full 3D dynamics [26]. One particular feature of the 1D model is that for unidirectional kicks ($\Delta p > 0$ or $\Delta p < 0$) two structurally different systems emerge [13,16]: When the kicks are directed towards the nucleus ($\Delta p < 0$), referred to in the following as negative kicks, the classical dynamics typically exhibits soft chaos with regular regions in phase space embedded in a chaotic sea. On the other hand, for the kicks directed away from the nucleus ($\Delta p > 0$, ''positive kicks''), the dynamics is globally chaotic even for infinitesimally small kick strength. The positively kicked Rydberg atom turns out to be, to some extent, more representative for the 3D case [26]. For reasons of comparison, we will also consider a sequence of alternating kicks,

$$V^A(t) = -q\Delta p\sum_{k=1}^{K} (-1)^k \delta\left(t - \frac{1}{2}\left(k - \frac{1}{2}\right)T\right). \tag{6}$$

This interaction resembles to some extent more closely the microwave driven Rydberg atom [13,14].

Due to the periodicity of the driving field, the solution of the time-dependent Schrödinger equation (TDSE)

$$i\frac{\partial}{\partial t}|\psi(t)\rangle = H(t)|\psi(t)\rangle \tag{7}$$

can be simply written as

$$|\psi(t = KT)\rangle = U(KT)|\psi(0)\rangle = [U(T)]^K|\psi(0)\rangle \tag{8}$$

in terms of the Floquet (or period-one evolution) operator $U(T)$. This Floquet operator consists of a product of the evolution operator $e^{-iH_{\rm at}t}$ of the unperturbed atom and the boost operator $e^{iq\Delta p}$, i.e.,

$$U(T) = e^{-iH_{\rm at}T/2}e^{iq\Delta p}e^{-iH_{\rm at}T/2}. \tag{9}$$

The problem is thus reduced to the evaluation of matrix elements of these two operators. In the numerical evaluation, the size of the basis is inevitably limited. Therefore, a set of basis functions has to be carefully chosen in order to evaluate both operators effectively and accurately.

In our previous studies we employed a set of Sturmian basis functions [15,16,27,28] within which the atomic Hamiltonian can be efficiently diagonalized and the free atomic evolution can be easily calculated. However, it is not straightforward to evaluate the boost operator in a Sturmian basis for large n [29]. On the other hand, grid-based methods employing localized basis functions are most suitable to evaluate the boost operator while causing difficulties for atomic Coulomb problems due to both the singularity at $q = 0$ and the long-range Coulomb distortion as $q \to \infty$. We therefore employ the generalized pseudospectral (GPS) method [30] using a basis defined by

$$H_{\rm at}|\phi_n\rangle = E_n|\phi_n\rangle \tag{10}$$

with boundary conditions $\phi_n(q=0) = 0$ and $\phi_n(q = Q^{max}) = 0$. The method combines two complementary methods in a hybrid form: The boost operator is evaluated on a grid in coordinate space while the free atomic evolution is evaluated in the pseudospectral basis,

$$\begin{aligned}\langle\phi_{n'}|U(T)|\phi_n\rangle &= \sum_{m',m}\int dq'\int dq\langle\phi_{n'}|e^{-iH_{\rm at}T/2}|\phi_{m'}\rangle \\ &\quad\times\langle\phi_{m'}|q'\rangle\langle q'|e^{iq\Delta p}|q\rangle\langle q|\phi_m\rangle \\ &\quad\times\langle\phi_m|e^{-iH_{\rm at}T/2}|\phi_n\rangle \\ &= \int dq e^{-iE_{n'}T/2}\langle\phi_{n'}|q\rangle e^{iq\Delta p}\langle q|\phi_n\rangle e^{-iE_nT/2}.\end{aligned} \tag{11}$$

For $n = 1,2,\ldots,n_c(\lesssim\sqrt{Q^{max}/2})$, the ϕ_n are the bound hydrogenic states with $E_n = -1/(2n^2)$. In addition, $|\phi_n\rangle$ for $n > n_c$ represent the continuum up to a cutoff energy $E_n \leq E_c$. Using the Legendre pseudospectral discretization of the spatial coordinate, both bound Rydberg and continuum states are well represented with a relatively small number of basis states. For example, wave functions including continuum states are very accurately represented using as little as two spatial grid points per half wave. We typically employ a number N of grid points $\{q_i; i = 1,\ldots,N\}$ with $0 < q_i < Q^{max}$ of the order of $N \approx 1300$ and $Q^{max} \approx 10^4$ a.u. This allows one to accurately represent Rydberg states up to $n \approx 70$ and continuum states up to $E_c \approx 0.02$ a.u. For such a

grid representation, the computationally efficient transformation from an energy to a coordinate representation $\langle q|\phi_n\rangle$ is easily achievable. A solution of the TDSE can be determined within a finite but large Hilbert space using the GPS method. However, spurious reflections at the border Q^{max} are inevitable. We therefore employ absorbing boundary conditions by multiplying the wave function with the masking function

$$g(q)=\frac{1}{1+\exp[(q-Q_c)/Q_l]} \tag{12}$$

in the grid basis after each kick. Q_c and Q_l are typically $0.8Q^{max}$ and $0.01Q^{max}$, respectively. In addition, there is a second class of reflections to be considered. As the kicks accelerate the electron to ''high'' energies (in relation to the initial binding energy), E can approach E_c which is implicitly defined by the grid spacing (by the maximum k_c representable by the grid). We therefore use an additional masking function for the pseudospectral basis,

$$\tilde{g}(E_n)=\frac{1}{1+\exp[(E_n-E_c)/E_l]} \tag{13}$$

with which ϕ_n is multiplied during each time-evolution with $E_l\approx 0.01E_c$. One period of the time-evolution is thus given by

$$\langle\phi_{n'}|U(T)|\phi_n\rangle=\int dq\sqrt{\tilde{g}(E_{n'})}e^{-iE_{n'}T/2}\langle\phi_{n'}|q\rangle \times g(q)e^{iq\Delta p}\langle q|\phi_n\rangle\sqrt{\tilde{g}(E_n)}e^{-iE_nT/2}. \tag{14}$$

As a result of the masking in coordinate space and energy space, the time evolution ceases to be unitary. It is nevertheless possible to achieve a proper representation of localization. One criterion for the latter is that the masking does not affect the localized part of the wave function within the finite Hilbert space. As an example we show in Fig. 1 the survival probability against ionization

$$P_{\rm sur}(t)=\sum_{n({\rm bound})}|\langle\phi_n|\psi(t)\rangle|^2 \tag{15}$$

as a function of time for different Q^{max}. Even when the norm of the entire wave function $\psi(t)$ (including its continuum portion) drastically varies, the survival probability remains stable as a function of Q^{max}. In other words, the masking eliminates a portion of the outgoing continuum wave without affecting the bound-state or localized portion.

For the analysis of the dynamics of high frequencies as well as comparison with other driven systems, it is useful to consider the Fourier analysis of the driving field for unidirectional kicks [Eq. (5)],

$$V(t)=F^{\rm av}q+2F^{\rm av}q\sum_{m=1}^{\infty}\cos\left[2\pi m\nu\left(t-\frac{T}{2}\right)\right]. \tag{16}$$

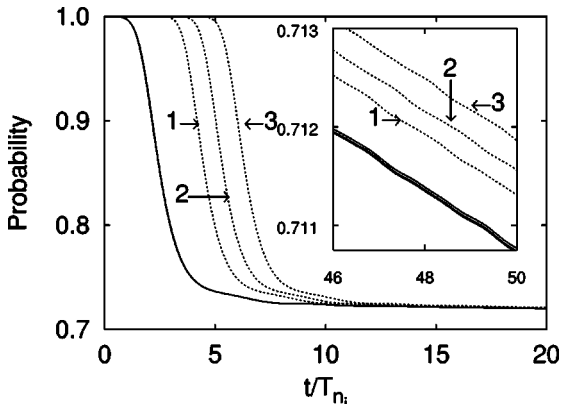

FIG. 1. Norm of the wave functions (dashed lines) and survival probabilities (full lines) for three choices of Q^{max} and N: (1) $Q^{max}=10^4$ a.u. and $N=1300$; (2) $Q^{max}=1.4\times10^4$ a.u. and $N=1700$, and (3) $Q^{max}=2\times10^5$ a.u. and $N=2500$. $\Delta p=7.5\times10^{-4}$ a.u., $n_i=20$ and $T=T_{n_i}/40=1.3\times10^3$ a.u. The survival probabilities for these three cases are practically identical. Inset: long-time behavior of norms and survival probabilities.

where $F^{\rm av}=-\Delta p/T$ and $\nu=1/T$. The train of pulses consists of a static (dc) field $F^{\rm av}$ and a multicolor driving field where all higher harmonics of the fundamental frequency ν are present with twice the amplitude $F^{\rm av}$ of the static field. The Hamiltonian can be accordingly decomposed as

$$H(t)=H_{\rm Stark}+2F^{\rm av}q\sum_{m=1}^{\infty}\cos\left[2\pi m\nu\left(t-\frac{T}{2}\right)\right] \tag{17}$$

with

$$H_{\rm Stark}=H_{\rm at}+qF^{\rm av}. \tag{18}$$

Correspondingly, for alternating kicks [Eq. (6)],

$$V^A(t)=4F^Aq\sum_{m=1}^{\infty}\cos\left[2\pi\nu(2m+1)\left(t-\frac{T}{4}\right)\right], \tag{19}$$

where $F^A=-\triangle p/T$ is the field of the odd Fourier components of the alternating field. Note that for alternating kicks T encompasses two kicks. The essential difference to Eq. (16) is the absence of the dc component which has profound consequences for the ensuing dynamics.

In the following sections we will use scaled units (i.e., measured in units of the initial Rydberg state), which we denote by the subscript ''0.'' The units are $t_0=t/(2\pi n_i^3)$, $\nu_0=2\pi n_i^3/T$, $q_0=q/n_i^2$, $p_0=pn_i$, $E_0=En_i^2$, and $F_0^{\rm av}=F^{\rm av}n_i^4$. Note that the classical dynamics in these units is invariant under a change of the action n_i.

III. QUANTUM LOCALIZATION IN THE HIGH-FREQUENCY LIMIT

We focus now on the quantum dynamics of the unidirectionally driven Rydberg atom [Eqs. (3),(4), and (5)] at high frequencies ν_0. By high we refer not only to $\nu_0\gg1$ but to $\nu_0\gtrsim n_i/2$ with $n_i\gg1$, i.e., frequencies sufficient already for

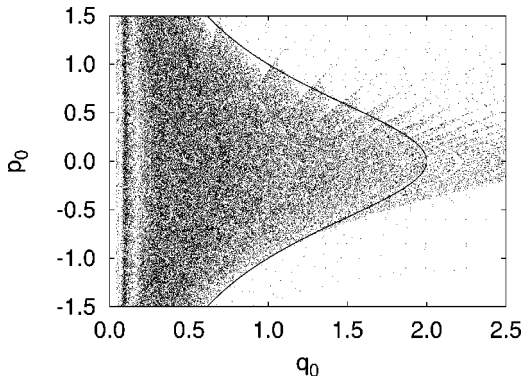

FIG. 2. Stroboscopic Poincaré surface of section for $\nu_0=21.1$ and positive unidirectional kicks with $F_0^{\mathrm{av}}=-0.095$. The line indicates the initial hydrogenic state. The stroboscopic snapshots are taken at $t_0=0,\ T_0,\ 2T_0,\ \ldots$.

the lowest Fourier component [Eq. (16)] of the driving field to induce photoionization by one-photon absorption. As the variables Δp_0 and F_0^{av} are interrelated with each other, we consider in the following variations of ν_0 at fixed F_0^{av} which implies that the kick strength

$$\Delta p_0=-2\pi F_0^{\mathrm{av}}/\nu_0 \tag{20}$$

scales inversely with ν_0. Moreover, the quiver amplitude for a system harmonically driven with the same frequency ν_0,

$$\alpha_0=(F_0^{\mathrm{av}})^2/(16\pi^2\nu_0^2), \tag{21}$$

which is a measure for the spatial strong-field excursion would scale as ν_0^{-2}. Regardless of the fact that the kicked system is not dynamically equivalent to the harmonically driven system, it is worth noting that we are concerned with the $\alpha_0\to 0$ regime; and the localization effects discussed in the following are different in origin of the strong-field high-frequency stabilization of harmonically driven systems [31,32]. To our knowledge, this regime of localization has not been previously investigated. The unidirectionally kicked atom is of particular interest as its classical phase space is globally chaotic without any stable island surviving and an algebraic decay of the dwell time distribution [13]. These features persist up to infinitely high frequencies, an example of which is displayed in Fig. 2 as the stroboscopic Poincaré surface of section for $\nu_0=21.1$. All tori are destroyed and, eventually, all trajectories undergo chaotic ionization. We note that the structure seen in the positive momentum part of the plot is a manifestation of the unstable manifold above the Stark barrier E_0^{barrier} where the density of points becomes discontinuously reduced due to strong ionization. Accordingly, the survival probability at a fixed interaction time is a measure for the transient stability and suppression of chaotic ionization.

Figure 3 shows the time evolution of the quantum and classical survival probabilities of the kicked Rydberg atom subject to a train of unidirectional kicks [Eq. (5)] as a function of scaled time. We use a hydrogenic state with $n_i=20$ as an initial state, the average field $F_0^{\mathrm{av}}=-0.095$, and two different frequencies of a train of pulses, $\nu_0=2.7$ (upper frame) and 15.5 (lower frame). Classical survival probabilities are evaluated using a classical trajectory Monte Carlo method with a microcanonical ensemble as an initial state [16,33]. They rapidly decay in contrast to the quantum survival probability. This suppression of classical chaotic ionization due to quantum interference effects is considered to be the hall mark of ''quantum localization'' in quantum systems corresponding to classically chaotic systems.

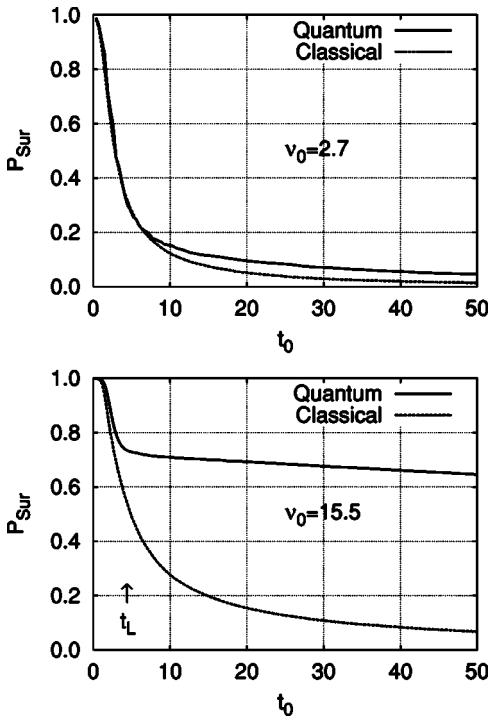

FIG. 3. Quantum and classical survival probabilities as a function of scaled time for two different frequencies ν_0 with $F_0^{\mathrm{av}}=-0.095$ and $n_i=20$. t_L denotes the localization time where the classical and quantum survival probabilities diverge from each other.

Complementary information on the phase space evolution is provided by the spectral distribution at fixed time t_0. The latter is defined by

$$\rho_0(E_{n,0},t_0)=\begin{cases}|\langle\phi_n|\psi(t_0)\rangle|^2/\Delta E_{n,0} & \text{(quantum)}\\ \displaystyle\int_{\tilde{E}_{n,0}<E<\tilde{E}_{n+1,0}} f(q,p,t_0)\,dqdp/\Delta E_{n,0} & \text{(classical)},\end{cases} \tag{22}$$

where $\tilde{E}_{n,0}=(E_{n-1,0}+E_{n,0})/2$, $\Delta E_{n,0}=(E_{n+1,0}-E_{n-1,0})/2$, and $f(q,p,t_0)$ is the classical phase space density distribution. Figure 4(a) indicates the initial distribution while Figs. 4(b) and 4(c) display the spectral distributions after 200 kicks corresponding to $t_0=12.9$. The energy distribution function obviously depends on the definition of the unperturbed Hamiltonian with respect to which the spectral distribution is determined. For the unidirectionally kicked atom, there are two physically meaningful choices: the zero-field

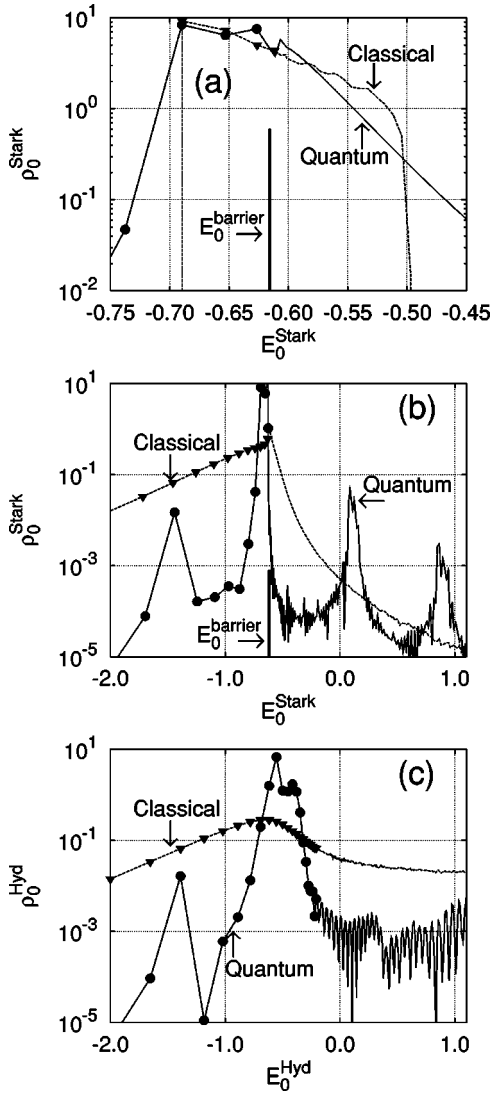

FIG. 4. The quantum and classical spectral densities $\rho_0(E_{n,0})$ with $n_i=20$, $F_0^{\mathrm{av}}=-0.095$, and $\nu_0=15.5$ as a function of the Stark energy [Eq. (18)]. (a) at $t=0$ (initial state); (b) after $K=200$ kicks. The same spectral density as in (b) is plotted in (c) but as a function of hydrogenic energy. The full lines in (a) and (b) indicate the energy $E_0^{barrier}$ of the Stark barrier.

Hamiltonian [Eq. (4)] used in Fig. 4(c) and the Stark Hamiltonian [Eq. (18)] including the dc field used in Figs. 4(a) and 4(b). When Eq. (22) is calculated for Stark energies $E_n=E_n^{\mathrm{Stark}}$ and Stark states, $|\phi_n^{\mathrm{Stark}}\rangle$, the initial state distribution is broadened [Fig. 4(a)] while it would be δ-shaped in the hydrogenic spectral distribution (not shown). Obviously one-photon ($m=1$) and two-photon ($m=2$) excitation peaks are much more pronounced in the Stark spectral distribution [Fig. 4(b)] since these ''photoionization'' events take place in the presence of a dc field while they are barely visible in the hydrogenic spectrum [Fig. 4(c)]. The classical spectral distribution is significantly broadened compared to the quantum distribution with enhancement both in the bound state spectrum (the latter being responsible for the algebraic long-time tail of the survival probability [13]) as well as in the above-barrier continuum which is responsible for the rapid classical ionization. The quantum spectrum shows both exponential localization around each photonic peak as well as power law localization for the envelope of the multiphotonic peak structure.

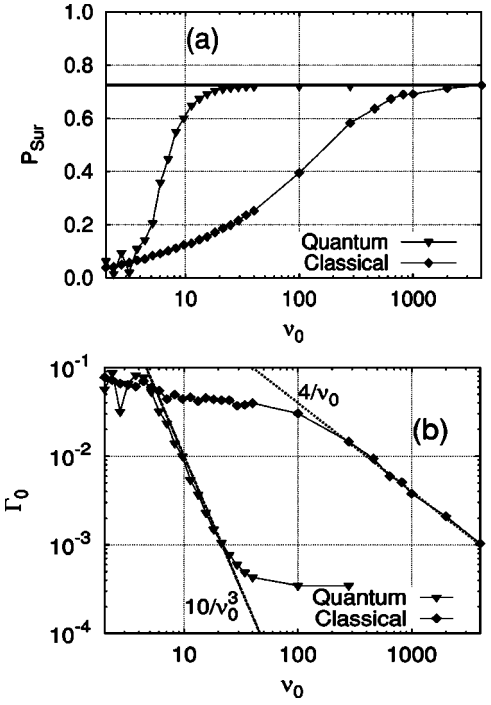

FIG. 5. Quantum and classical survival probabilities (a) and scaled decay rates (b) as a function of scaled frequency. The data are taken at $t_0=20$ with $F_0^{\mathrm{av}}=-0.095$ and $n_i=20$.

The dependence on high driving frequencies is displayed in Fig. 5. The survival probability at fixed scaled evolution time $t_0=20$ shows the persistence of quantum localization up to very high frequencies $\nu_0\approx 1000$. Unlike the microwave ionization problem [5,24], classical stochastic ionization dominates over quantum ''photoionization'' even for $\nu_0 \gg n_i/2$. The classical and quantum survival probabilities in Fig. 5(a) appear to approach the same value of $P_{\mathrm{sur}}\approx 0.72$ with increasing ν_0. This is a peculiar feature for short to intermediate interaction times and high frequencies for the unidirectionally kicked atom. Increasing t_0 at fixed ν_0 results in additional features to be discussed below. Due to the presence of an average field F_0^{av}, the ionization threshold is lowered to the height of the saddle of the potential barrier $E_0^{\mathrm{barrier}}=-2\sqrt{\Delta p_0/(2\pi T_0)}=-2\sqrt{-F_0^{\mathrm{av}}}$ displayed in Figs. 4(a) and 4(b). Since a hydrogenic state is used as an initial state in the simulation, the initial distribution in the Stark basis [Fig. 4(a)] is broad and a finite fraction of the initial probability resides above E_0^{barrier}. The ionization at high kick frequencies *and* short interaction times can be understood as the depletion of the fraction of the initial population residing above the Stark barrier. Also in this regime, the quantum ionization is suppressed compared to the classical counterpart up to very high frequencies. This difference is more clearly visible in the scaled decay rate $\Gamma_0(t_0)$ defined as the logarithmic derivative

$$\Gamma_0(t_0)=-\dot{P}_{\mathrm{sur}}(t_0)/P_{\mathrm{sur}}(t_0). \tag{23}$$

where a dot indicates a derivative with respect to t_0. Classical decay rates remain orders of magnitude larger up to high frequencies [Fig. 5(b)]. The behavior of Γ_0, both classically and quantum mechanically, can be understood in terms of simple physical arguments. A typical lifetime of the classical system is the average time it takes for the trajectories to absorb an amout of energy equal to the binding energy. Hence the classical decay rate can be estimated from the ratio of the average energy gain per scaled unit time $\langle \Delta \dot{E}_0 \rangle$ to the energy $\Delta E_0^I = E_0^{\text{barrier}} - E_{n_i,0}$ necessary to reach the barrier,

$$\Gamma_0^{\text{cl}} = \langle \Delta \dot{E}_0 \rangle / (\Delta E_0^I). \tag{24}$$

Since ΔE_0^I is dependent only on F_0^{av} and is independent of ν_0, the only ν_0 dependence in Eq. (24) originates from $\langle \Delta \dot{E}_0 \rangle$. The energy gain per kick is given by

$$\langle \Delta E_0 \rangle_{\text{kick}} = \frac{\Delta p_0^2}{2} + \langle p_0 \rangle \Delta p_0 . \tag{25}$$

The energy gain per scaled unit time is

$$\langle \Delta \dot{E}_0 \rangle = \nu_0 \langle \Delta E_0 \rangle_{\text{kick}} . \tag{26}$$

As an electron with $E_0 < 0$ travels around the nucleus, the average momentum cancels out (i.e., $\langle p_0 \rangle \approx 0$) since p_0 has different signs if the electron is traveling towards or away from the nucleus. Therefore Eqs. (24) and (26) lead to the scaling

$$\Gamma_0^{\text{cl}} \approx \langle \Delta \dot{E}_0 \rangle \approx 1/\nu_0 \tag{27}$$

since $\Delta p_0 \propto 1/\nu_0$ [Eq. (20)]. This behavior is, indeed, observed well into the regime where the survival probability has reached the value predicted by the initial fraction of underbarrier population, i.e., Eq. (27) applies also to the slow classical diffusive ionization of the underbarrier population giving rise to the power-law tail in P_{sur}. We note that this scaling law differs from the prediction by Hillermeier *et al.* using the Fokker-Planck equation [13]. This is due to the fact that in our case the process is not well-approximated by the Fokker-Planck equation since the high frequency perturbation with weak kick strength does not strongly randomize the process until the electron is scattered by the nucleus.

The quantum decay rate is, for intermediate frequencies $\nu_0 \approx n_i/2$, characterized by a rapid decay $\sim \nu_0^{-3}$ [Fig. 5(b)]. This behavior can be easily understood as follows: The *exact* evolution operator for the unidirectionally kicked Rydberg atom [Eq. (9)] can be visualized as the *approximate* discretized prescription within the split-operator algorithm [34] of the time evolution generated by the Hamiltonian with a time-independent external field [Eq. (18)] with a discretization step $\delta t = T \propto 1/\nu_0$. This method is known to converge to order $O(\delta t^3) \sim O(\nu_0^{-3})$. This is precisely the slope seen in Fig. 5(b). However, for larger ν_0 we observe a leveling-off indicating the appearance of a new regime. As will be discussed below the regime of large ν_0 is governed by zero-frequency Stark tunneling.

IV. QUENCHING OF LOCALIZATION BY STARK TUNNELING

In order to analyze the long-time evolution and quantum localization in more detail, it is convenient to study the Floquet spectrum, i.e., the eigenstates and eigenvalues of the period-one evolution operator [25],

$$U(T) |\phi_k^F\rangle = e^{-i\mathcal{E}_k T} |\phi_k^F\rangle, \tag{28}$$

where $\mathcal{E}_k = \mathcal{E}_k^R - \imath \mathcal{E}_k^I$ are the complex quasi-eigenenergies. The imaginary part of $\mathcal{E}_k$ is related to the decay rates Γ_0 discussed above. This relation is the key to the description of quantum localization: Quantum dynamics is unitary in the full Hilbert space $\mathcal{H}$. Only by restricting the dynamics to a subspace $\mathcal{P} \subset \mathcal{H}$ the Floquet eigenvalues obtain a finite imaginary part $\mathcal{E}_k^I$. The restriction in the present case corresponds to the projective elimination of outgoing continuum waves by masking [Eqs. (12) and (13)]. In other words, the complement $\mathcal{Q}$ of $\mathcal{P}$ corresponds to a subspace of the continuum spectrum not subtended by the present pseudospectral grid. Conversely, true bound states as well as Floquet states representing completely localized wave packets in the continuum (resonances with infinite lifetimes) should reside in $\mathcal{P}$ and should have zero imaginary parts. Provided that the basis set spanning up $\mathcal{P}$ is large enough to represent any physical backscattering towards the nucleus and the masking functions are smooth enough to prevent spurious reflections at the border through high Fourier components, the flux going out of the basis corresponds to a physical flux rather than a numerical artifact. Small $\mathcal{E}_k^I$ of Floquet states living mainly in the bound space can then be given the physical interpretation of decay widths of quasi-stable Floquet states in the kicked Rydberg atom, whose inverse lifetimes in scaled units are $\tau_{k,0}^{-1}/2 = 2\pi n_i^3 \mathcal{E}_k^I$. Floquet states with either zero or very small $\mathcal{E}_k^I$ can therefore be used as one (not necessarily unique) indicator of quantum localization. In practice, $\mathcal{E}_k^I$ cannot be exactly zero. Considering exponential localization in energy space around a fixed energy E_m, the probability for occupying a pseudo-spectral basis state with energy E is given by

$$P(E) \sim e^{-|(E-E_m)|/E_L}, \tag{29}$$

where E_L is the localization length in energy space. There is thus a small but finite probability for reaching the border of $\mathcal{P}$ in energy space,

$$P(E_c) \sim e^{-(E_c - E_m)/E_L} > 0 \tag{30}$$

and hence a small probability for escaping $\mathcal{P}$ and reaching $\mathcal{Q}$ leading to $\mathcal{E}_k^I > 0$. This is closely related to the so-called ''atomic conductance'' [22] in analogy to quantities used in mesoscopic devices.

It is now instructive to analyze the behavior of the lifetimes of the Floquet states at large ν_0 and to understand their

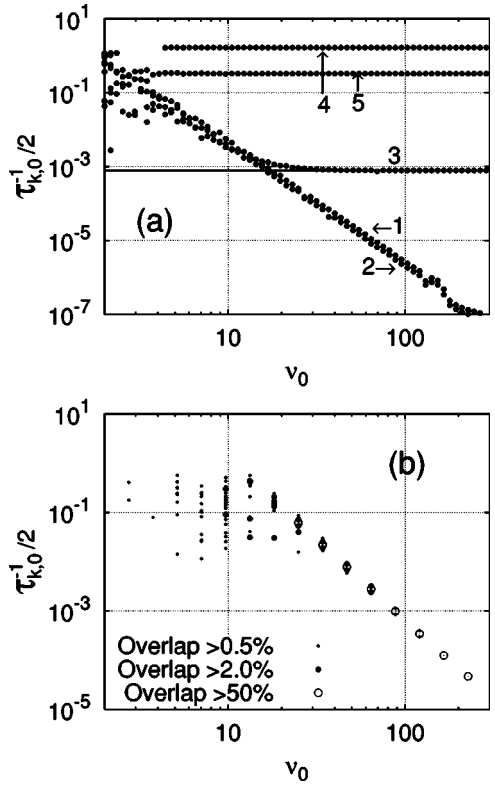

FIG. 6. The inverse scaled lifetime $\tau_{k,0}^{-1}$ of the Floquet states for $n_i=20$ as a function of scaled frequency: (a) unidirectional kicks with $F_0^{\mathrm{av}}=-0.095$ [Eq. (5)] and (b) alternating kicks with $F_0=-0.5$ [Eq. (6)]. At each frequency we plot several Floquet states whose overlap probability with the initial state $|\langle\phi_{n_i}|\phi_k^F\rangle|^2$ is larger than 5% (a) and 0.5% (b). In (a), the data are numbered according to descending order of overlap and the solid line corresponds to the inverse lifetime of the dc Stark state with $E_0^{\mathrm{Stark}}=-0.62$ in Fig. 4(a). Note that only one state in (b) carries almost all of the probability for large ν_0 and that no other state has a probability larger than 0.5% above $\nu_0=150$.

implication for quantum localization. In Fig. 6 we contrast the behavior of $\tau_{k,0}^{-1}$ for a few dominant Floquet states with the largest probability in the initial state for both unidirectional and alternating kicks. For alternating kicks [Fig. 6(b)], $\tau_{k,0}^{-1}$ decays for high frequencies as ν_0^{-3}. The same applies to the case of unidirectional kicks [Fig. 6(a)], but only for intermediate values of ν_0, in agreement with the trends observed for Γ_0 (see Fig. 5). For higher frequencies, the inverse lifetimes begin to level off at small but finite values and approach a constant. In other words the scaled lifetime t_0^D of localization is limited due to a constant ''leakage'' rate of the Floquet state given by the saturation value of $\tau_{k,0}^{-1}$. This leakage eventually destroys the quantum localization. The quantum localization for the unidirectionally and positively kicked atom is therefore characterized by two different time scales: a localization time t_0^L where classical and quantum dynamics separate and localization sets in as quantum interferences suppress classical ionization (Fig. 3) and a much longer decay (or decoherence) time t_0^D where quantum localization is eventually destroyed.

It is now of interest to inquire into the origin of the decay of the localized state. The Fourier decomposition of the Hamiltonian [Eq. (17)] suggests that the high-frequency decay is determined by the zero-frequency Stark Hamiltonian, i.e., the *static* field ionization process. In order to support this interpretation, we have performed complex-scaling calculations [35] for the one-dimensional Rydberg atom in the presence of a dc Stark field (shown as a full line in Fig. 6). We find for the dominant states with the largest overlap with the initial state excellent agreement between the imaginary part of the Floquet eigenvalue of the full dynamical problem [all Fourier components of Eq. (17) included] with the imaginary part of the static field problem [Eq. (18)]. This agreement immediately implies that these Floquet states should closely resemble Stark eigenstates in the dc field.

Since the initial Rydberg state displays a broad distribution in the spectral density calculated for Stark states [Fig. 4(a)], the high frequency limit of the unidirectionally kicked atom corresponds to several Floquet states resembling the different Stark states overlapping with the initial state, as seen in Fig. 6(a). For the alternating kicks, on the other hand, the time-independent part of the Hamiltonian [Eq. (6)] is the atomic Hamiltonian [Eq. (4)]. Therefore, in the high-frequency limit, the time-evolution of the wave function converges towards just one Floquet state resembling the initial Rydberg state, as can be seen in Fig. 6(b) for $\nu_0>150$. We thus arrive at the remarkable conclusion that states representing the high-frequency limit of quantum localization are given by the time-independent part of the Hamiltonian which for alternating kicks is the Rydberg Hamiltonian and for unidirectional kicks is the zero-frequency *Stark* Hamiltonian.

V. CLASSICAL STARK ORBITS AND QUANTUM LOCALIZATION

In order to analyze the connection between the high-frequency localization and the dc Stark problem further, we analyze the classical-quantum correspondence of the problem. The skeleton of the classically chaotic phase space is provided by unstable periodic orbits (UPOs). Figure 7(a) shows two typical UPOs for the kicked Rydberg atom with a fixed average field and two different driving frequencies. As ν_0 increases, the UPOs begin to resemble a Stark orbit. Already for $\nu_0=21$, the similarity between the UPO and the Stark orbit is striking. In Fig. 7(b), on the other hand, we show a typical chaotic classical trajectory. The initial conditions are almost the same as those for the UPO with $\nu_0=21$, but q_0 is shifted by $\Delta q_0=0.007$. This trajectory does not correspond to a certain Stark orbit, but at each impact with the nucleus it jumps from one Stark orbit to another until it eventually ionizes. The key point is now that quantum mechanics ''smears out'' the classical phase space structure rendering the quantum evolution insensitive to the instability of the classical trajectory. To quantify the role of the uncertainty principle in stabilizing the quantum phase space flow, we measure the deviation of an UPO from a Stark orbit by taking a difference in action $\Delta S=\oint|p_{\mathrm{Stark}}(q)-p_{\mathrm{UPO}}(q)|dq$. We consider the difference in action averaged over one-period T, i.e., $\langle\Delta S\rangle=\Delta S/K$ as a measure for the distance in action space. For $\langle\Delta S\rangle\ll\hbar$ the quantum system cannot ''re-

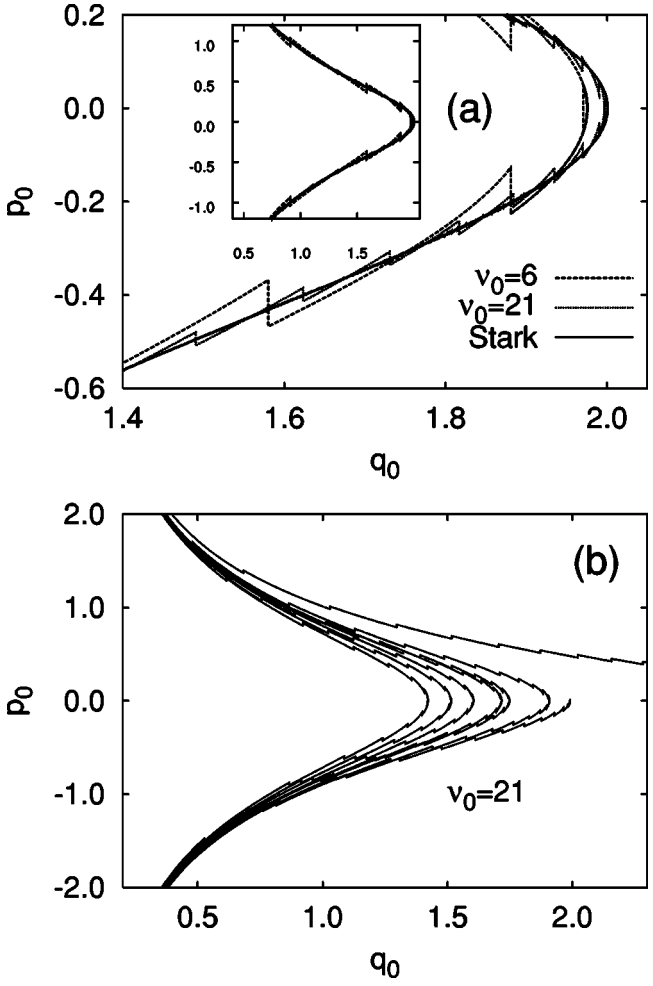

FIG. 7. (a) Classical unstable periodic orbits (UPOs) and a corresponding Stark orbit ($F_0^{\mathrm{av}}=-0.095$). (b) Typical classical trajectory launched in the vicinity of the UPO of (a).

solve'' the difference between a Stark orbit and a UPO and, therefore, the quantum evolution will retrace the Stark orbit which, in turn, corresponds to the fact that the Floquet states converge to Stark states. On the other hand, for $\langle \Delta S \rangle \gg \hbar$ the quantum evolution will ''feel'' the difference between the

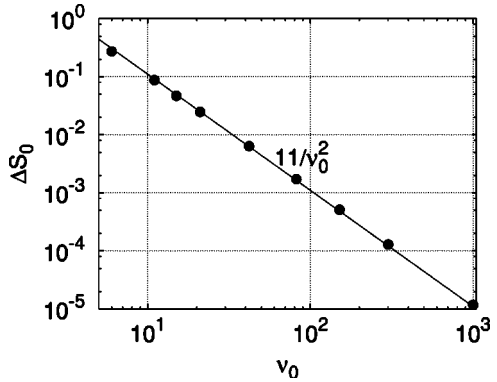

FIG. 8. The average difference in scaled action $\langle \Delta S_0 \rangle$ between unstable periodic orbits and a Stark orbit: Numerical simulations (symbols) are fitted by $11/\nu_0^2$ (solid line).

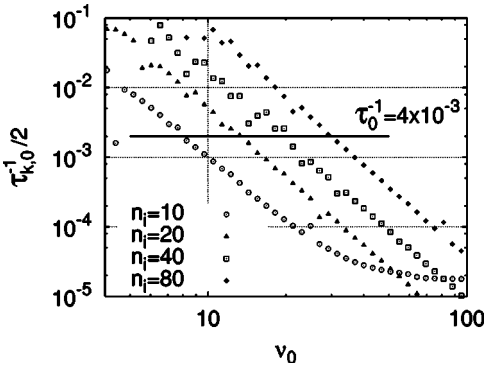

FIG. 9. Scaled inverse lifetimes $\tau_{k,0}^{-1}/2$ of the dominant Floquet state with the largest probability in the initial state for $F_0^{\mathrm{av}}=-0.095$ and different initial states ($n_i=10,20,40,80$). The horizontal line indicates a lifetime $\tau_0^{-1}=4\times10^{-3}$.

UPO and the Stark orbit and will contribute to rapid decay and ionization. Figure 8 shows the numerically evaluated scaled $\langle \Delta S_0 \rangle = \langle \Delta S \rangle / n_i$ as a function of ν_0. In order to observe quantum localization, the scaled difference in action $\langle \Delta S_0 \rangle$ must be smaller than a critical value ΔS_0^c which is of the order of the scaled Planck's constant, $\Delta S_0^c \ll \hbar_0 = 1/n_i$. From Fig. 8 we can read off the scaling relation

$$\langle \Delta S_0 \rangle \approx 11/\nu_0^2 \ll \frac{1}{n_i}. \tag{31}$$

Equation (31) implies that the critical scaled frequency ν_0^{crit} for the onset of high-frequency localization scales as

$$\nu_0^{\mathrm{crit}} \propto n_i^{0.5}. \tag{32}$$

This prediction can be tested against the numerical data for the unidirectionally kicked Rydberg atom. We consider the scaled inverse lifetime $\tau_{k,0}^{-1}$ of the dominant Floquet state as a function of ν_0 for different n_i (Fig. 9). A well-localized state that has converged towards the Stark state is characterized by a small $\tau_{k,0}^{-1}$. Setting an ''arbitrary'' threshold for the lifetime (e.g., $\tau_{k,0}^{-1} \approx 4\times10^{-3}$, thick solid line in Fig. 9) we can determine the scaling relation for $\nu_0(n_i)$ from the points

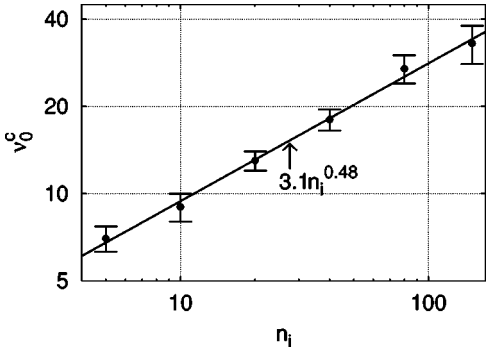

FIG. 10. Points of intersection between $\tau_0^{-1}=4\times10^{-3}$ and $\tau_{k,0}^{-1}$ as a function of n_i (Fig. 9). Note that both axes are plotted in logarithmic scale. The error bars at each n_i are estimated by intersections with different Floquet states [see Fig. 6(a)].

of intersection between the horizontal line with the curves $\tau_{k,0}^{-1}$ for different n_i. The resulting relation is practically independent of the specific choice of the threshold value. We find $\nu_0^{\mathrm{crit}} \propto n_i^{0.48}$ (Fig. 10) in good agreement with the estimate of Eq. (32). These findings support the proposition that the difference between the UPO and a Stark orbit controls the frequency regime above which the localization in the high-frequency regime sets in.

VI. SUMMARY

We have studied the quantum localization of the periodically kicked Rydberg atom in the limit of high frequencies for a fixed average field strength. We find that localization, that is, the quantum suppression of classically chaotic ionization, persists up to very high frequencies well into the photoionization regime. Moreover, the high-frequency Floquet states converge to Stark states. We have presented a semiclassical argument explaining this convergence in terms of the proximity of unstable orbits to Stark states for small but finite $\hbar$. Several properties of high-frequency Floquet states can be deduced from zero-frequency Stark states, most notably, the lifetime of dc Stark states against tunneling ionization determines the upper bound for the time scale over which quantum localization can be observed.

ACKNOWLEDGMENTS

This work was supported by the FWF and FWF-SFB 016 (Austria). C.R. acknowledges support by U.S. DOE OBES, DCS managed by UT-Battelle, LLC under Contract No. DE-AC05-00OR22725.

[1] H. Friedrich and D. Wintgen, Phys. Rep. **183**, 37 (1989).
[2] C. H Iu, G. R Welch, M. M Kash, L. Hsu, and D. Kleppner, Phys. Rev. Lett. **63**, 1133 (1989).
[3] G. Casati, B.V. Chirikov, F.M. Izraelev, and J. Ford, Lect. Notes Phys. **93**, 334 (1979).
[4] S. Fishman, D.R. Grempel, and R.E. Prange, Phys. Rev. Lett. **49**, 509 (1982).
[5] P. Koch and K. Van Leeuwen, Phys. Rep. **255**, 290 (1995).
[6] J.E. Bayfield and L.A. Pinnaduwage, Phys. Rev. Lett. **54**, 313 (1985).
[7] G. Casati, B.V. Chirikov, D.L. Shepelyansky, and I. Guarneri, Phys. Rep. **154**, 77 (1987); R.V. Jensen, S.M. Susskind, and M.M. Sanders, *ibid.* **201**, 1 (1991); S.M. Susskind and R.V. Jensen, Phys. Rev. A **38**, 711 (1988).
[8] J. Leopold and D. Richards, J. Phys. B **22**, 1931 (1989).
[9] R.R. Jones, D. You, and P.H. Bucksbaum, Phys. Rev. Lett. **70**, 1236 (1993).
[10] M.T. Frey, F.B. Dunning, C.O. Reinhold, and J. Burgdörfer, Phys. Rev. A **53**, R2929 (1996).
[11] A. Dhar, M. Nagaranjan, F. Izrailev, and R. Whitehead, J. Phys. B **16**, L17 (1983); A. Carnegie, *ibid.* **17**, 3435 (1984).
[12] J. Burgdörfer, Nucl. Instrum. Methods Phys. Res. B **42**, 500 (1989); M. Melles, C.O. Reinhold, and J. Burgdörfer, *ibid.* **79**, 109 (1993).
[13] C.F. Hillermeier, R. Blümel, and U. Smilansky, Phys. Rev. A **45**, 3486 (1992).
[14] G. Casati, I. Guarneri, and G. Mantica, Phys. Rev. A **50**, 5018 (1994); H. Wiedemann, J. Mostowski, and F. Haake, *ibid.* **49**, 1171 (1994).
[15] C.O. Reinhold, M. Melles, and J. Burgdörfer, Phys. Rev. Lett. **70**, 4026 (1993); J. Phys. B **26**, L659 (1994).
[16] C.O. Reinhold, J. Burgdörfer, M.T. Frey, and F.B. Dunning, Phys. Rev. Lett. **79**, 5226 (1997); M.T. Frey, F.B. Dunning, C.O. Reinhold, S. Yoshida, and J. Burgdörfer, Phys. Rev. A **59**, 1434 (1999).
[17] M. Klews and W. Schweizer, Phys. Rev. A **64**, 053403 (2001).
[18] J. Ahn, D.N. Hutchinson, C. Rangan, and P.H. Bucksbaum, Phys. Rev. Lett. **86**, 1179 (2001); T.J. Bensky, M.B. Campbell, and R.R. Jones, *ibid.* **81**, 3112 (1998).
[19] C. Wesdorp, F. Robicheaux, and L.D. Noordam, Phys. Rev. Lett. **87**, 083001 (2001); C. Wesdorp, F. Robicheaux and L.D. Noordam, Phys. Rev. A **60**, 5122 (1999).
[20] P.W. Anderson, Phys. Rev. **109**, 1492 (1958); Rev. Mod. Phys. **50**, 191 (1978).
[21] F.L. Moore, J.C. Robinson, C.F. Bharucha, B. Sundaram, and M.G. Raizen, Phys. Rev. Lett. **75**, 4598 (1995).
[22] A. Buchleitner and D. Delande, Chaos, Solitons Fractals **5**, 1125 (1995); S. Wimbergerer and A. Buchleitner, J. Phys. A **34**, 7181 (2001).
[23] S. Yoshida, C.O. Reinhold, and J. Burgdörfer, Phys. Rev. Lett. **84**, 2602 (2000).
[24] D. Richards, in *Classical, Semiclassical and Quantumdynamics in Atoms*, Lecture Notes in Physics, Vol. 485, edited by H. Friedrich and B. Eckart (Springer, New York, 1997), p. 173.
[25] J.H. Shirley, Phys. Rev. **138**, B979 (1965).
[26] E. Persson *et al.* (unpublished).
[27] M. Rotenberg, Adv. At. Mol. Phys. **6**, 233 (1970).
[28] S. Yoshida, C.O. Reinhold, P. Kristöfel, and J. Burgdörfer, Phys. Rev. A **62**, 023408 (2000).
[29] Dž Belkić, J. Phys. B **14**, 1907 (1981); I. Bersons and A. Kulsh, Phys. Rev. A **55**, 1674 (1997).
[30] X.M. Tong and S.I. Chu, Chem. Phys. **217**, 119 (1997); J. Wang, S.I. Chu, and C. Laughlin, Phys. Rev. A **50**, 3208 (1994).
[31] M. Gavrila, *Atoms in Intense Laser Fields* (Academic Press, London, 1992).
[32] B. Sundaram and R.V. Jensen, Phys. Rev. A **47**, 1415 (1993).
[33] R. Arbines and I.C. Percival, Proc. Phys. Soc. **88**, 861 (1966).
[34] M.D. Feit, J.A. Fleck, and A. Steiger, J. Comput. Phys. **47**, 412 (1982).
[35] B. Simon, Int. J. Quantum Chem. **14**, 529 (1978).